JPE 19-3-15

https://doi.org/10.6113/JPE.2019.19.3.771
ISSN(Print): 1598-2092 / ISSN(Online): 2093-4718

SynRM Driving CVT System Using an ARGOPNN with MPSO Control System

Chih-Hong Lin† and Kuo-Tsai Chang*

†,*Department of Electrical Engineering, National United University, Miaoli, Taiwan

Abstract

Due to nonlinear-synthetic uncertainty including the total unknown nonlinear load torque, the total parameter variation and the fixed load torque, a synchronous reluctance motor (SynRM) driving a continuously variable transmission (CVT) system causes a lot of nonlinear effects. Linear control methods make it hard to achieve good control performance. To increase the control performance and reduce the influence of nonlinear time-synthetic uncertainty, an admixed recurrent Gegenbauer orthogonal polynomials neural network (ARGOPNN) with a modified particle swarm optimization (MPSO) control system is proposed to achieve better control performance. The ARGOPNN with a MPSO control system is composed of an observer controller, a recurrent Gegenbauer orthogonal polynomial neural network (RGOPNN) controller and a remunerated controller. To insure the stability of the control system, the RGOPNN controller with an adaptive law and the remunerated controller with a reckoned law are derived according to the Lyapunov stability theorem. In addition, the two learning rates of the weights in the RGOPNN are regulating by using the MPSO algorithm to enhance convergence. Finally, three types of experimental results with comparative studies are presented to confirm the usefulness of the proposed ARGOPNN with a MPSO control system.

Key words: Continuously variable transmission, Gegenbauer orthogonal polynomials neural network, Particle swarm optimization, Synchronous reluctance motor

I. INTRODUCTION

With the use of optimal design methods [1], [2], synchronous reluctance motors (SynRMs) have a high power factor, high efficiency and low torque ripple when compared with the induction motors (IMs). In addition, they have been widely applied in the fluid movement and textile applications, such as water well pumps and fiber spinning machines [3], [4].

V-belt continuously variable transmission (CVT) systems [5]-[8] are mostly applied in motorcycles and cars. They are frequently composed of a V-belt chain and two sets of pulleys with two springs. A CVT system can be driven in any speed operation when the radii of the two sets of pulleys are changed. Thus, the operated speed of a CVT system is controlled by use of an alternating current (AC) machine is mainly studied motivated by use of CVT dynamics and nonlinear control schemes. Guzzella et al. [5] proposed a normal proportional-integral-derivative (PID) controller with measurements of the gear ratio to adjust the speed of CVT-based vehicles. Kim et al. [6] proposed a fuzzy logic controller to control the speed of a CVT system. However, some added load and parameter variations tests as well as the simplified model of a CVT system controlled by the use of a SynRM have yet to be demonstrated in any studies. Thus, this study will demonstrate the simplified model of a CVT system controlled by using a SynRM and control.

A lot of artificial neural networks (NNs) can realize a wide variety of nonlinear identification and dynamic controls [9], [10] owing to their improved learning capability. In addition, function-link NNs [11]-[14] were proposed to cut down computational complexity. Moreover, to save computing costs and to reduce longer iterative-training procedures, the good approximation capability of parameters by use of a Gegenbauer polynomials neural networks (GOPNNs) [15], [16] has been proposed. Nevertheless, the previous feedforward NNs may not efficiently process the dynamic properties of a system. Thus, recurrent Gegenbauer polynomials neural networks (RGOPNNs) [17]-[19] with a better approximated capacity and learning behavior have been proposed. However, these NNs may need longer computing time due to the inadequate regulation of some of the learning rates. To reduce

Manuscript received Oct. 13, 2018; accepted Feb. 6, 2019
Recommended for publication by Associate Editor Dong-Hee Lee.
†Corresponding Author: jhlin@nuu.edu.tw
Tel: +886-3-7382464, Fax: +886-3-7382468
*Dept. of Electrical Engineering, National United University, Taiwan

longer computational times, various kinds of the optimal methods have been used to regulate learning rates.

The particle swarm optimization (PSO) proposed by Kennedy et al. [20] is a kind of self-regulation grabble optimal skill. PSO acts on the societal conduct of particles in a group. Hence, it seeks out the global best solution via regulating the trajectory of every particle toward its own best position and toward the best particle of the whole group at each step [20], [21]. Meanwhile, PSO has been broadly applied in mathematic modeling and functional optimization [22]-[24] due to its easier fulfillment and faster convergence toward the best solution. In an effort to avoid premature convergence of the PSO, Lin et al. [19] proposed adaptive particle swarm optimization (APSO) with an adaptive inertia weight and an adaptive constriction factor to adjust the two learning rates of the weights in the RGOPNN for a SynRM driving CVT system. However, the adaptive dynamic inertia weight and adaptive constriction factor varied with the step *t*. As a result, this method leads to a lower convergence speed. Thus, a modified particle swarm optimization (MPSO) with a fixed-dynamic inertia weight and a fixed-dynamic constriction factor can result in faster convergence due to the upper-lower limitation of the convergence range.

An admixed recurrent Gegenbauer orthogonal polynomials neural network (ARGOPNN) with a MPSO control system has been proposed to control SynRM driving CVT systems with a lot of nonlinear dynamics [25]-[27]. The ARGOPNN with a MPSO control system has a better dynamic response and a faster convergence than the blend RGOPNN with an APSO control system [19] or the blend modified RGOPNN control system [17], [18] with artificial bee colony optimization (ABCO). The ARGOPNN with a MPSO control system involves observer control, RGOPNN control and remunerated control. In order to assure stability of the control system, the weights of the RGOPNN control, which are regulated by using an adaptive law, and the remunerated control, which is regulated by using a reckoned law, are computed by means of the Lyapunov stability theorem. Likewise, to enhance the convergence of the parameters in the RGOPNN, a M*PSO algorithm* is adopted for adjusting the two types of learning rates. Finally, the effectiveness of control performance of the ARGOPNN with a MPSO control system is confirmed by experimental results.

This paper is organized as follows. Section II presents the composition of the SynRM driving CVT system. Section III presents the design method of the ARGOPNN with a MPSO control system. Section IV presents some experimental results. Section V provides a number of conclusions.

II. Depiction of the System

The complete system of the SynRM driving CVT system is made up of four systems, which are a CVT system, a SynRM driving system, a field-oriented control system, and a speed/

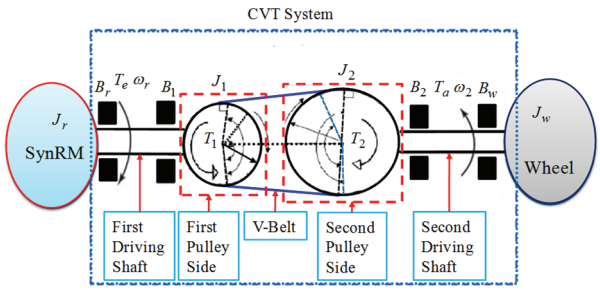

Fig. 1. Compendium diagram of a CVT system.

torque control system. Fig. 1 shows a compendium diagram of a CVT system. Simplified models of the torque dynamics in the first driving side and the second driven side of the CVT are presented by [5]-[8]:

$$T_e = J_1\dot{\omega}_r + B_1\omega_r + T_1 \tag{1}$$

$$T_2 = J_a\dot{\omega}_2 + B_a\omega_2 + T_a \tag{2}$$

Hence, by means of the speed ratio and the sliding ratio [5]-[8] between the second pulley side and the first pulley side, the torque equation can be converted into a combined dynamic equation. When the transmission power loss, slip loss and belt flexural effects are neglected, the combined dynamic equation [5]-[8] of the SynRM driving CVT system by use of (1) and (2) can be presented by:

$$T_e = T_1^l + J_b\,\dot{\omega}_r + B_b\,\omega_r \tag{3}$$

where $T_1 = \sigma_2 T_2$ denotes the identical driving torques in the first pulley side. σ_2 denotes the transposition ratio between the first pulley side and the second pulley side. T_2 denotes the identical driven torque in the second pulley side. J_w, J_2, $J_a = J_w + J_2$, J_1, J_r and $J_b = J_1 + J_r$ denote the moment of inertia of the wheel, the moment of inertia of the first pulley shaft, the sum moment of inertia of the second shaft-wheel side, the moment of inertia of the second shaft, the moment of inertia of the SynRM, and the sum moment of inertia of the first pulley shaft-SynRM side, respectively. B_w, B_2, $B_a = B_w + B_2$, B_1, B_r and $B_b = B_1 + B_r$ denote the viscous friction coefficient of the wheel, the viscous friction coefficient of the first pulley shaft, the sum viscous friction coefficient of the second shaft-wheel side, the viscous friction coefficient of the second shaft, the viscous friction coefficient of the SynRM, and the sum viscous friction coefficient of the first pulley shaft-SynRM side, respectively. $T_a = T_a^l(v_a, \tau_a, F_a, B_a, \omega_2)$ denotes the total nonlinear extrinsic disturbances, which are composed of the wind obstruction τ_a, the braking force F_a, and the rolling obstruction v_a. In additon, ω_2 and ω_r denote the mechanical angular speed of the second pulley shaft and the mechanical angular speed of the rotor in the SynRM, respectively. $T_1 = T_1^l + J_r\,\dot{\omega}_r + B_r\omega_r$ is the identical driving torque in the first pulley side. $T_1^l = \sigma_2(J_a\dot{\omega}_2 + B_a\omega_2 + T_a) = \Delta T + T_l + T_t$ [5]-[8] indicates the total nonlinear extrinsic disturbances and parameter variations. $T_t = F_l(B_a) + \upsilon_a(v_2, B_a) + \tau_a(v_2)\omega_2^2$,

$\Delta T = \Delta J_r \dot{\omega}_r + \Delta B_r \omega_r$, and T_l are the total unknown nonlinear load torque, the total parameter variation, and the fixed load torque, respectively. $F_l(B_a)$, $\upsilon_a(v_2, B_a)$ and $\tau_a(v_2)$ are the total braking force, the total rolling resistance, and the total wind resistance, respectively.

The SynRM driving system is made up of interlock and isolated circuits and a voltage source inverter (VSI) with three-sets of insulated-gate bipolar transistor (IGBT) power modules.

The field-oriented control system is made up of a $\sin\theta_f / \cos\theta_f$ generation, a lookup table generation, a proportional-integral (PI) current control, a coordinate transformation system with an inverse coordinate transformation, and a sinusoidal pulse-width-modulation (PWM) control modulator. The admix signal field-programmable-gate-array (FPGA) system by means of a Xilinx Spartan-XCS10XL chip; where its norm is 80 MHz, 6,272 distributed RAM bits, 10,000 gates, 616 flip-flops, and 112 input/output (I/O) ports; was applied to execute the field-oriented control. The *d*-axis and *q*-axis models of the SynRM in the synchronous rotating frame [3], [4] can be expressed by:

$$v_{qt} = R_t\, i_{qt} + L_{qt}\, \dot{i}_{qt} + P\,\omega_r L_{dt}\, i_{dt} / 2 \tag{4}$$

$$v_{dt} = R_t\, i_{dt} + L_{dt}\, \dot{i}_{dt} - P\,\omega_r L_{qt}\, i_{qt} / 2 \tag{5}$$

where R_t denotes the stator resistance, i_{dt} and i_{qt} denote the *d*-axis and *q*-axis stator currents, v_{dt} and v_{qt} denote the *d*-axis and *q*-axis stator voltages, L_{dt} and L_{qt} denote the *d*-axis and *q*-axis stator inductances, and P is the number of poles. The electromagnetic torque [3], [4] of the SynRM driving CVT system can be expressed by:

$$T_e = 3P\,[(L_{dt} - L_{qt})\, i_{dt}\, i_{qt}]/4 \tag{6}$$

The prime theory for controlling a SynRM is adopted by the field orientation using the constant *d*-axis current. As a result, the electromagnetic torque T_e is directly proportional to i_{qt}, which is determined by closed-loop control. Furthermore, when the torque angle is $\pi/4$ [3], [4] and the *d*-axis rotor flux is equal to the *q*-axis rotor flux, the maximum torque per ampere can be achieved.

The speed/torque control system is executed by using a digital signal processor (DSP) control system. The DSP control system by means of a Texas Instrument (TI) TMS320F28335 MCU; where its norm is 150 MHz, 256K×16 bits Flash RAM, 34K×16 bits SARAM, 16 sets of channels analog-digital converters (ADC) with 12 bits, 18 sets of programmable-PWM ports, 6 sets of high-resolution PWM ports, and 2 sets of quadrature encoder interfaces; was applied to complete the speed/torque control. The two control parameters of the PI current controller are rendered by $k_{ci} = k_{cp}/T_{ci} = 5.62$ and $k_{cp} = 10.8$ via some heuristic lore [26]-[28] to acquire a better dynamic response. The fabric of the SynRM driving CVT system is shown in Fig. 2.

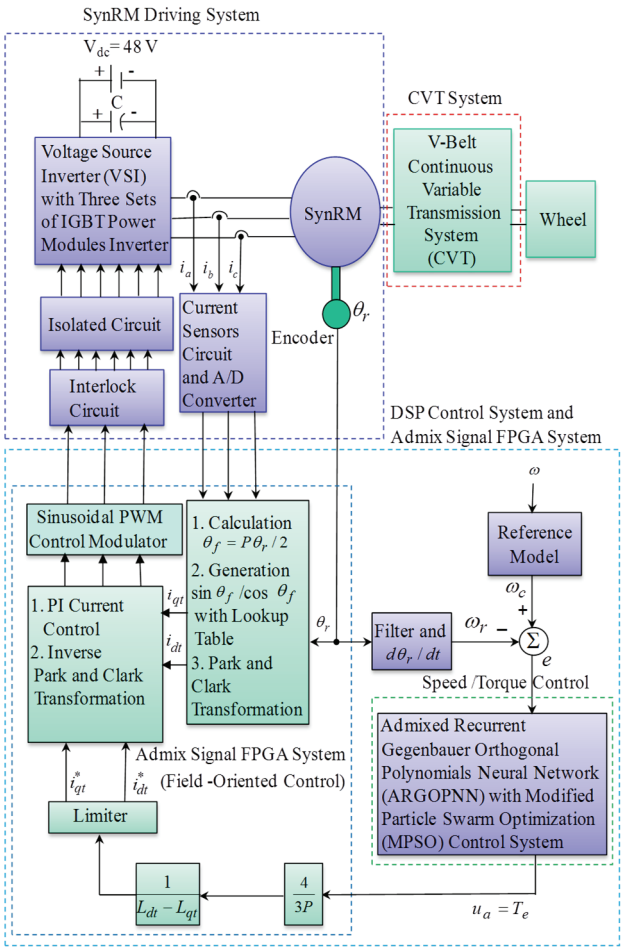

Fig. 2. Fabric of the SynRM driving CVT system.

III. ARGOPNN WITH A MPSO CONTROL SYSTEM

By using (3), the dynamic equation of the SynRM driving CVT system is denoted by:

$$\dot{\omega}_r = A_a\omega_r + A_b u_a + A_c(\Delta T + T_l + T_t) \tag{7}$$

Then the tracking error e is defined by:

$$e = \omega_c - \omega_r \tag{8}$$

where $u_a = T_e$ is the mandate torque of the SynRM. In addition, $A_a = -B_r/J_r$, $A_b = 1/J_r$ and $A_c = -1/J_r$ are the three known constants. ω_c is the expected command rotor speed. All of parameters are assumed to be bounded under the occurrence of uncertainties as well as known. Hence, the perfect control law is denoted by:

$$u_a^* = [\dot{\omega}_c + k_a e - A_a\omega_r - A_c(\Delta T + T_l + T_t)]/A_b \tag{9}$$

where k_a is a positive constant. By using (9) and replacing $u_a^* = u_a$ into (7), the error dynamic equation is given by:

$$\dot{e} + k_a e = 0 \tag{10}$$

If $e(t) \to 0$ as $t \to \infty$ in (10), the system state gradually tracks the expected trajectory.

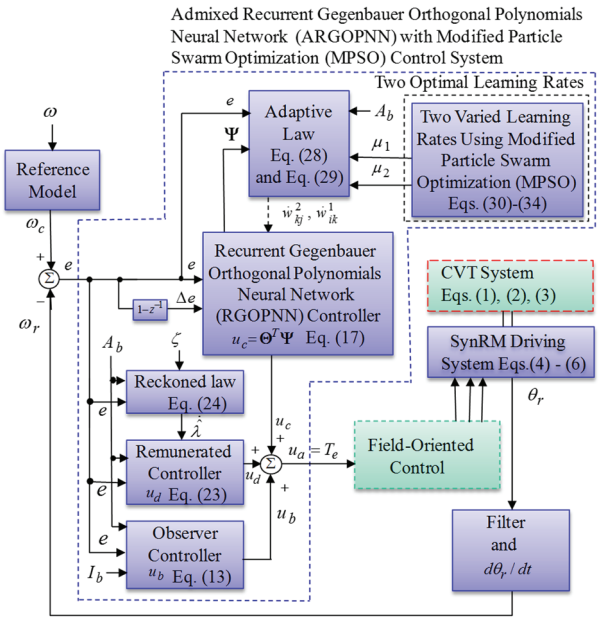

Fig. 3. Fabric of the ARGOPNN with a MPSO control system.

A. ARGOPNN with a MPSO Control System

The fabric of the ARGOPNN with a MPSO control system illustrated in Fig. 3 is used to impersonate the perfect control law. The control effort of the ARGOPNN with a MPSO control system is designed by:

$$u_a = u_b + u_c + u_d \tag{11}$$

where u_b is the observer controller, u_c is the RGOPNN controller, and u_d is the remunerated controller. With differential (8) and by using (7), (9), (10) and (11), the error dynamic equation can be acquired by:

$$\dot{e} = -k_a e + [u_a^* - u_b - u_c - u_d]A_b \tag{12}$$

B. Observer Controller

The observer control u_b is given by:

$$u_b = I_b \operatorname{sgn}(eA_b)[D_1(\omega_r) + D_2 + |\dot{\omega}_c| + |k_a e|]/A_b \tag{13}$$

where $\operatorname{sgn}(\cdot)$ is a sign function.

C. RGOPNN Controller

The RGOPNN controller u_c is the output of the three-layer RGOPNN. The fabric of the three-layer RGOPNN [15], [16] is illustrated in Fig. 4, which is comprised of an input, a hidden layer and an output layer. The input and output signals for the input, hidden and output layers can be denoted by:

$$y_i^1 = f_i^1(\prod_k x_i^1(N) w_{ik}^1 y_k^3(N-1)), \quad i = 1, 2 \tag{14}$$

$$y_j^2 = G_j^\sigma(\sum_{i=1}^{2} y_i^1(N) + \beta\, y_j^2(N-1)), \ j = 0, 1, \cdots, l-1 \tag{15}$$

$$y_k^3 = f_k^3(\sum_{j=0}^{m-1} w_{kj}^2 y_j^2(N)), \quad k = 1 \tag{16}$$

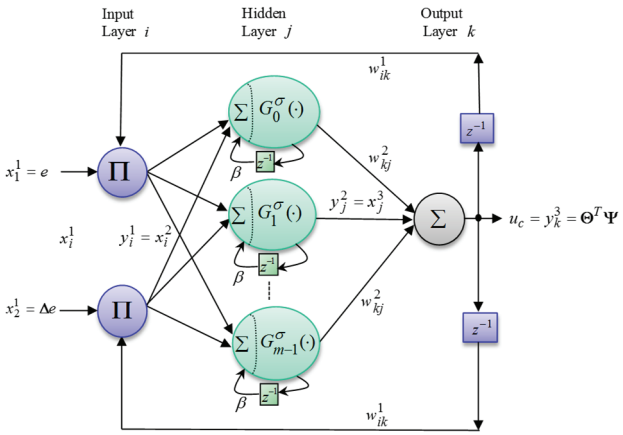

Fig. 4. Fabric of a three-layer RGOPNN.

where $x_1^1 = \omega_c - \omega_r = e$ denotes the tracking error of the rotor speed, and $x_2^1 = e(1 - z^{-1}) = \Delta e$ denotes the tracking error variation. w_{ik}^1 and w_{kj}^2 denote the recurrent weight from the output layer to the input layer, and the connective weight from the hidden layer to the output layer, respectively. N denotes the number of iterations. Gegenbauer orthogonal polynomials (GOPs) $G_n^\sigma(x)$ [15]-[19] present the argument of polynomials with $-1 < x < 1$, where σ and n are the number of order and the order of expansion, respectively. m denotes the number of nodes in the hidden layer. β denotes the self-connecting feedback gain of the hidden layer with $0 < \beta < 1$. The zero, first and second orders GOPs can be represented by $G_0^\sigma(x) = 1$, $G_1^\sigma(x) = 2\sigma x$ and $G_2^\sigma(x) = 2x^2(\sigma+1)\sigma - \sigma$, respectively. The higher order GOPs $G_n^\sigma(x) = [2(n+\sigma-1)xG_{n-1}^\sigma(x) - (n+2\sigma+2)G_{n-2}^\sigma(x)]/n$ can be generated by the recursive formula. f_i^1 and f_k^3 are all of the linear activation functions. The output u_c of the RGOPNN controller can be denoted by:

$$u_c = y_k^3(N) = \begin{bmatrix} w_{10}^2 & \cdots & w_{1,l-1}^2 \end{bmatrix} \begin{bmatrix} x_0^3 & \cdots & x_{l-1}^3 \end{bmatrix}^T = \Theta^T \Psi \tag{17}$$

where $\Theta = \begin{bmatrix} w_{10}^2 & \cdots & w_{1,m-1}^2 \end{bmatrix}^T$ denotes the vector of weights from the hidden layer to the output layer. $\Psi = \begin{bmatrix} x_0^3 & \cdots & x_{m-1}^3 \end{bmatrix}^T$ denotes the vector of inputs in the output layer.

D. Remunerated Controller

The affinity error δ can be denoted by:

$$\rho = u_a^* - u_c^* = u_a^* - (\Theta^*)^T \Psi \tag{18}$$

where Θ^* denotes the vector of the perfect weight toward the minimum affinity error. In general, a small positive number λ is greater than the absolute value of ρ, i.e., $\lambda > |\rho|$. By using (17) and (18), it is possible to denote (12)

as:

$$\dot{e} = -k_1 e + [\rho + (\boldsymbol{\Theta}^* - \boldsymbol{\Theta})^T \boldsymbol{\Psi} - u_d - u_b] A_b \tag{19}$$

By using the Lyapunov function $L_a(t)$, it is possible to denote $L_a(t)$ as:

$$L_a(t) = e^2/2 + (\boldsymbol{\Theta}^* - \boldsymbol{\Theta})^T (\boldsymbol{\Theta}^* - \boldsymbol{\Theta})/(2\mu_1) + \tilde{\lambda}^2/(2\zeta) \tag{20}$$

where $\tilde{\lambda} = \hat{\lambda} - \lambda$ denotes the reckoned error with a limit. ζ denotes the adaptive gain. μ_1 denotes the leaning rate. By differentiating (20) with respect to t and using (19), it is possible to rewrite (20) as:

$$\dot{L}_a(t) = \{-k_a e^2 + [\rho - u_d - u_b] A_b e + (\boldsymbol{\Theta}^* - \boldsymbol{\Theta})^T \boldsymbol{\Psi} A_b e - (\boldsymbol{\Theta}^* - \boldsymbol{\Theta})^T \dot{\boldsymbol{\Theta}}/\mu_1 + \tilde{\lambda}\dot{\hat{\lambda}}/\zeta \tag{21}$$

The adaptive law $\dot{\boldsymbol{\Theta}}$ can be denoted by:

$$\dot{\boldsymbol{\Theta}} = \mu_1 \boldsymbol{\Psi} A_b e \tag{22}$$

The remunerated controller u_d with a reckoned law $\dot{\hat{\lambda}}$ can be denoted by:

$$u_d = \hat{\lambda}\,\mathrm{sgn}(A_b e) \tag{23}$$

$$\dot{\hat{\lambda}} = \zeta\,\mathrm{sgn}(A_b e) \tag{24}$$

Substituting (13) with $I_b = 0$, (22), (23) and (24), it is possible to obtain (21) by:

$$\dot{L}_a(t) \le -k_a e^2 + \{|\rho| - \lambda\}|A_b e| \le -k_a e^2 \le 0 \tag{25}$$

Let $\upsilon(t) = -\dot{L}_a(t) = k_a e^2$ be a uniformly continuous function. Then $\dot{L}_a(t)$ is a negative semi-definite, i.e., $L_a(t) \le L_a(0)$. This makes e and $(\boldsymbol{\Theta}^* - \boldsymbol{\Theta})$ bounded. By use of Barbalat's lemma [25, 26], $\lim_{t\to\infty} \upsilon(t) = 0$, i.e., $e(t) \to 0$ as $t \to \infty$.

E. Weight Training of the RGOPNN

An online weight training method for the RGOPNN can be invented and skilled in accordance with the Lyapunov stability theorem. By using the adaptive law $\dot{\boldsymbol{\Theta}}$ denoted in (22), the adaptive law of the connective weight w_{kj}^2 is given by:

$$\dot{w}_{kj}^2 = \mu_1 y_j^2 A_b e \tag{26}$$

A cost function, which is an important index in the online training algorithm of the RGOPNN, can be denoted by:

$$V_a = e^2/2 \tag{27}$$

Then the adaptive law of connective weight by means of gradient descent technology can be computed by:

$$\dot{w}_{kj}^2 = -\mu_1 \frac{\partial V_a}{\partial w_{kj}^2} = -\mu_1 \frac{\partial V_a}{\partial y_k^3}\frac{\partial y_k^3}{\partial w_{kj}^2} = -\mu_1 \frac{\partial V_a}{\partial y_k^3} y_j^2 \tag{28}$$

When compared to (26) and (28), equation (28) produces $\partial V_a / \partial y_k^3 = -e A_b$. The adaptive law of recurrent weight w_{ik}^1 by means of gradient descent technology can be computed by:

$$\dot{w}_{ik}^1 = -\mu_2 \frac{\partial V_a}{\partial w_{ik}^1} = \mu_2 A_b\, e\, w_{kj}^2 G_j^{\sigma}(\cdot) x_i^1(N) y_k^3(N-1) \tag{29}$$

where μ_2 denotes the learning rate.

F. MPSO Algorithm

To the find two optimized learning rates of the two weights in the RGOPNN, a MPSO is proposed. A flowchart of resulting two optimized learning rates by using the MPSO algorithm is shown Fig. 5. The MPSO algorithm [19], [22], [24] is given by:

$$\mu_{m,n}(t+1) = \mu_{m,n}(t) + v_{m,n}(t+1),\ m = 1, 2,\ n = 1, \cdots, l_1 \tag{30}$$

$$v_{m,n}(t+1) = \gamma_m(t) v_{m,n}(t) + g_{m,n}(t+1),\ m = 1, 2,\ n = 1, \cdots, l_1 \tag{31}$$

$$g_{m,n}(t+1) = \alpha_m(t)[k_{m1}\varphi_1(P_{m,n}^b - \mu_{m,n}(t)) + k_{m2}\varphi_2(P_{m,n}^g - \mu_{m,n}(t))],\quad m = 1,\ 2,\ n = 1,\ \cdots,\ l_1 \tag{32}$$

$$\gamma_m(t) = \begin{cases} \gamma_{m,\min} + \dfrac{\varphi_3(\gamma_{m,\min} - \gamma_{m,\max})(z_m - z_{m,\min})}{(z_{m,avg} - z_{m,\min})}, & \text{if } z_m \le z_{m,\min},\ m = 1,2 \\ \gamma_{m,\max}, & \text{if } z_m > z_{m,avg},\ m = 1,2 \end{cases} \tag{33}$$

$$\alpha_m(t) = \begin{cases} \dfrac{\alpha_{m0}}{\dfrac{(k_{m1} + k_{m2})}{2} - 1 + \sqrt{\dfrac{(k_{m1} + k_{m2})^2}{4} - (k_{m1} + k_{m2})}}, & (k_{m1} + k_{m2}) \ge 4,\ m = 1,2 \\ \alpha_{m0}, & 0 < (k_{m1} + k_{m2}) < 4,\ m = 1,2 \end{cases} \tag{34}$$

where $\mu_{m,n}(t)$ is the current position of particle $P_{m,n}$ in the nth hyperspace at step t, with regard to the optimized learning rate $\mu_m(t)$, $m = 1,2$ at step t. In addition, $v_{m,n}(t)$, $m = 1,2$ is the current speed of particle $P_{m,n}$. Furthermore, $\gamma_m(t), m = 1, 2$ is the inertia weight within $0.4 < \gamma_{m,n}(t) < 0.9$ [19]-[24] at step t. Therefore, the found space can be altered steadily from global to local. $\gamma_{m,\min}$ and $\gamma_{m,\max}$ represent the minimum value and maximum value of the inertia weight $\gamma_m(t)$. Meanwhile, k_{m1} and k_{m2} are two acceleration constants that are greater than zero. φ_1, φ_2 and φ_3 are three random numbers by means of a uniform random distribution function between 0 and 1. $P_{m,n}^b$ and $P_{m,n}^g$ represent the best previous position of the nth hyperspace and the position of the best particle among all of the particles in the nth hyperspace, respectively. z_m is the current aim function value of the particles. $z_{m,avg}$, $z_{m,\max}$ and $z_{m,\min}$ are the average aim function value, the maximum aim function value and the minimum aim function value in all of the current particles, respectively. α_{m0} is the initial positive constant in the interval [0, 1]. $\alpha_m(t)$ is the constriction

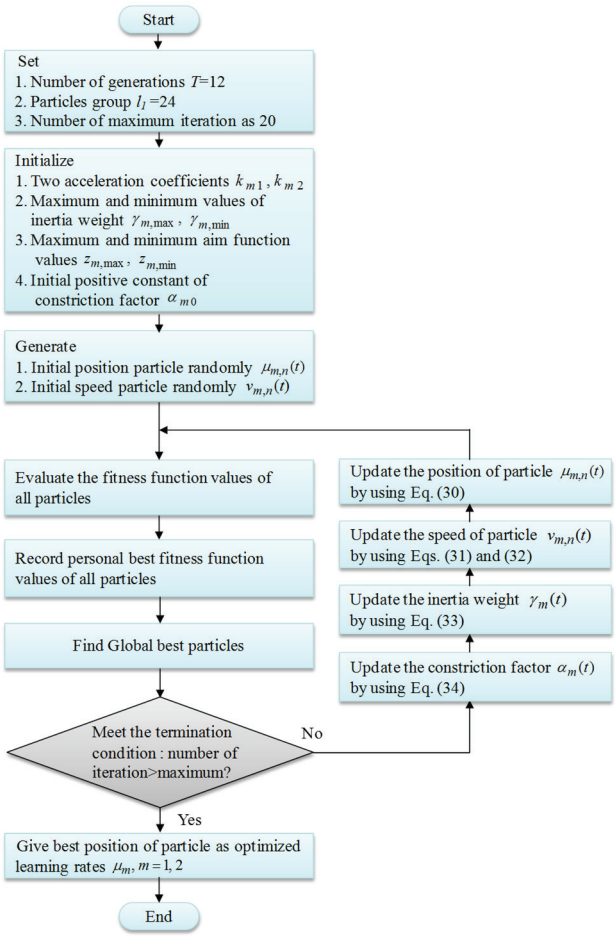

Fig. 5. Flowchart of the resulting two optimized learning rates by using a MPSO algorithm.

factor [19], [24] to avoid the swarm from premature convergence and to ensure the stability of the system. k_{m1}, k_{m2} and the inertia weight $\gamma_m(t), m=1,2$ in the PSO can have in an important effect on the performance of the algorithm. A larger inertia weight results ia a slower convergence and works well in global searches. A smaller inertia weight results in a faster convergence and reaches a more accurate optimal value. However, this only works well in local searches. In summary, the online tuning algorithm of the RGOPNN is based on the adaptive laws (28) and (29) for the weight adjustments by using the optimized learning rates $\mu_{m,n}(t) = \mu_m^*(t),\ m=1,2$ in (30). Moreover, the RGOPNN weights estimation errors are basically bounded [40]. The RGOPNN weight estimation errors are bounded to ensure that the control signal is bounded.

IV. Experimental Results

The fabric of a SynRM driving CVT system by means of a DSP control system is shown in Fig. 2. All of the mechanical and electrical parameters of the SynRM can be expressed by

TABLE I
Specifications of the SynRM and Drives

Specifications of the SynRM	
Number of phases	3
Rated voltage [V]	48
Rated current [A]	35
Rated speed [r/min]	3600
Power factor	0.86
Rated power [kW]	1.5
Number of poles	2
Number of rotor flux-*barrier layers*	3
Number of stator slots	24
Frequency [Hz]	60
Specifications of the Drive	
IGBT power modules	MACMIC-MMG100S060B6EN
Driving method	Sinusoidal PWM
Operated frequency [kHz]	15kHz

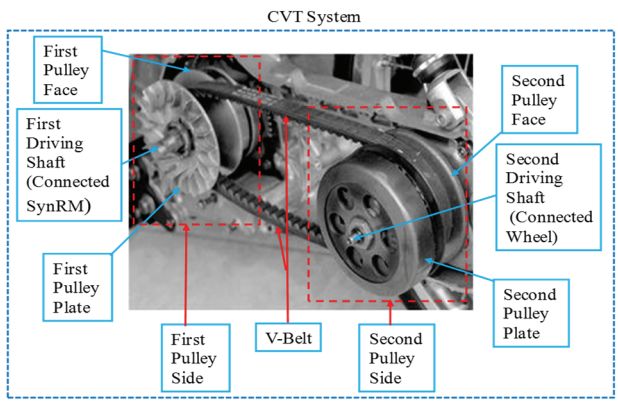

(a)

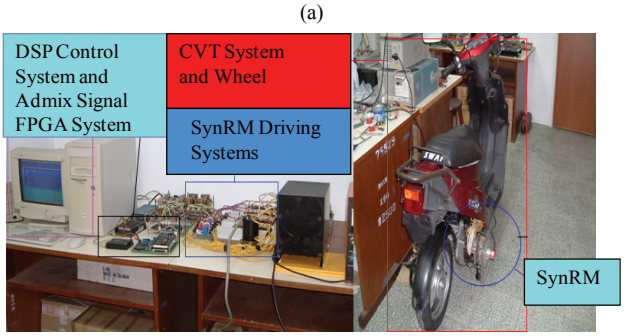

(b)

Fig. 6. Images of the experimental setup. (a) CVT system. (b) SynRM driving CVT system.

$J_r = 1.21\times10^{-3}\,Nms^2$, $B_r = 3.42\times10^{-3}\,Nms/rad$, $R_t = 0.92\Omega$, $L_{qt} = 23.22\,mH$ and $L_{dt} = 148.72\,mH$. The specifications of the SynRM and drives used for the experiment are shown in Table I. The SynRM driving CVT system can be rigged under total nonlinear uncertainties and extrinsic torque disturbances. An image of the experimental setup is shown in Fig. 6.

To demonstrate the control performance of the proposed method, two test cases are provided in the experiment. Case 1

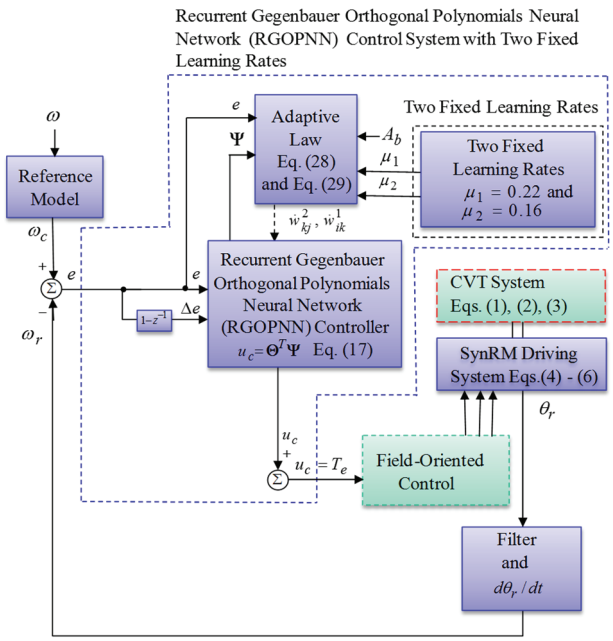

Fig. 7. Fabric of the RGOPNN control system with two fixed learning rates.

is working on a total unknown nonlinear load torque and one parameter variation $T_1^l = \Delta T + T_t$ from 0 */min* to 1800 *r/min* (188.4 *rad/s*). Case 2 is working on a total unknown nonlinear load torque and two parameters variations $T_1^l = 2\Delta T + T_t$ from 0 *r/min* to 3600 *r/min* (376.8 *rad/s*).

Considering the prerequisite of stability, the control gains of the recurrent Gegenbauer orthogonal polynomials neural network (RGOPNN) control system with two fixed learning rates are given as $\mu_1 = 0.22$ and $\mu_2 = 0.16$ to achieve the best transient control performance. The numbers of the neurons of the input-hidden-output layers in the RGOPNN shown in Fig. 4 are 2-4-1. The fabric of the RGOPNN control system with two fixed learning rates is illustrated in Fig. 7.

A flowchart of the execution of the RGOPNN control system with two fixed learning rates and real-time implementation by use of a DSP control system consisting of a chief program and an interrupt routine program (IRP) is shown in Fig. 8. Some of the parameters and input/output (I/O) ports are initialized in the chief program. Then the interrupt interval with a 2 *ms* sampling interval for the interrupt routine program (IRP) is set. After that, the interrupt is enabled. Some control data are then monitored by use of the chief program. The IRP is applied to read the rotor position of the SynRM driving CVT system from the encoder interface and the three-phase currents from the analog-to-digital (A/D) converter. It also has to calculate rotor position and speed, execute the lookup table, coordinate the translation, execute the PI current control, execute the RGOPNN control system with two fixed learning rates, and output the three-phase current commands to the sinusoidal PWM circuit

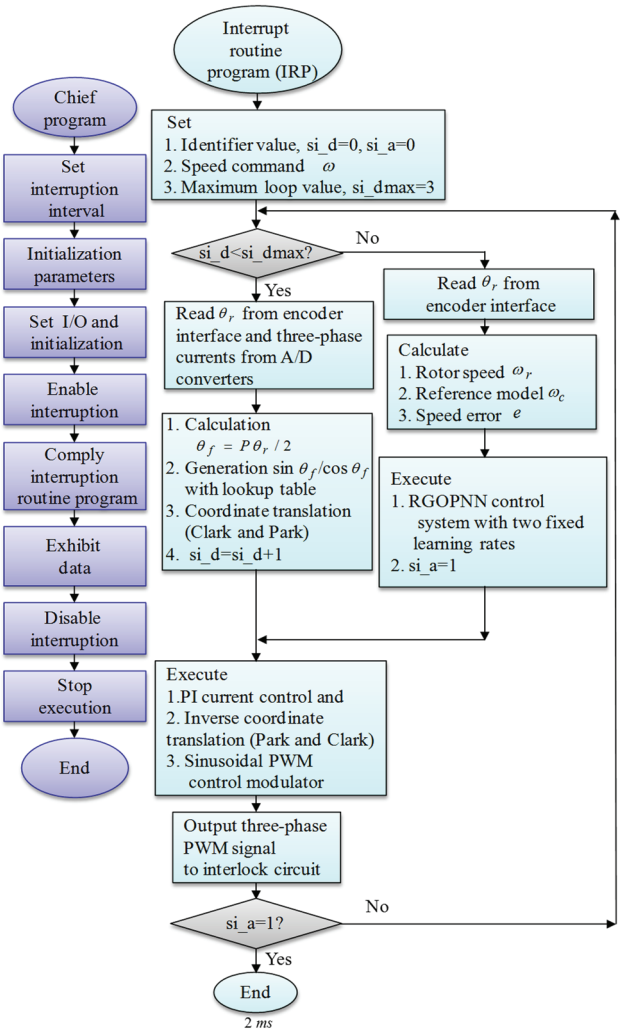

Fig. 8. Flowchart of the RGOPNN control system with two fixed learning rates by means of a DSP control system.

for switching the 3-sets of IGBT power modules VSI via interlock and isolated circuits. The 3-sets of IGBT power modules VSI is switched by the current-controlled sinusoidal PWM modulator with a switching frequency of 15 kHz.

Experimental results under Case 1 and Case 2 using the RGOPNN control system with the two fixed learning rates for the SynRM driving CVT system are shown in Fig. 9 and Fig. 10, respectively.

Fig. 9(a) shows the best tracking performance among the command rotor speed ω, desired command rotor speed ω_c and measured rotor speed ω_r under the low speed operation condition due to low disturbances. Fig. 10(a) shows an obvious degeneration of the tracking response of the speed under high velocity operation due to increases in nonlinear disturbances, i.e., friction and rolling resistances. Fig. 9(b) and Fig. 10(b) show larger tracking errors. Fig. 9(c) and Fig. 10(c) show a lot of vibration in the responses of the electromagnetic torque T_e. Fig. 9(d) and Fig. 10(d) illustrate the poor tracking responses of the command current i_a^* and

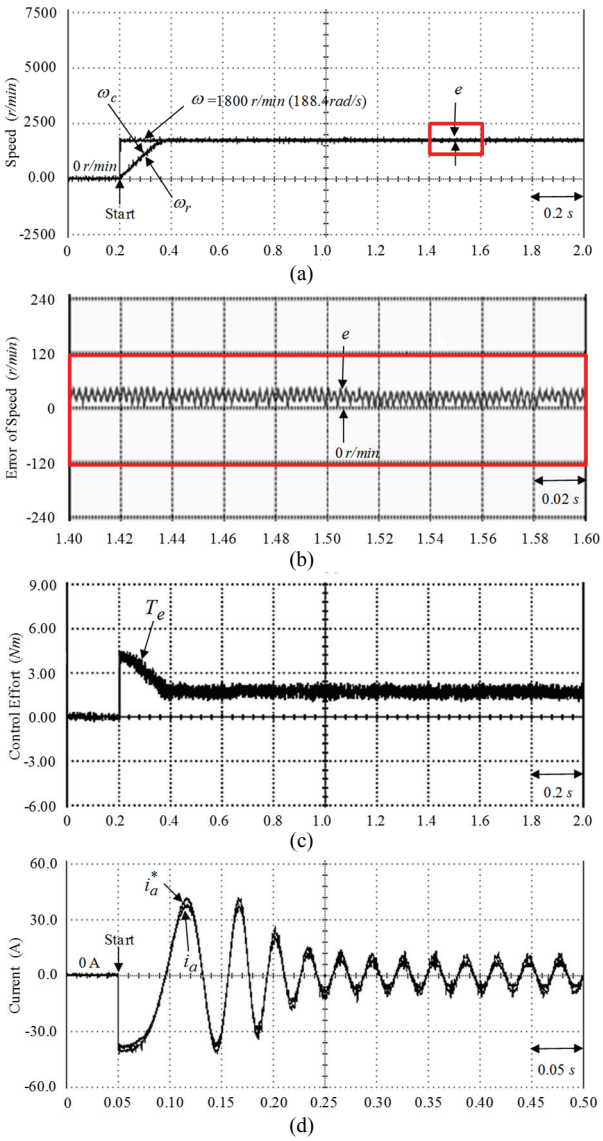

Fig. 9. Experimental results of the RGOPNN control system with two fixed learning rates for the SynRM driving CVT system in Case 1. (a) Tracking response of the rotor speed. (b) Zoomed response of the tracking error e. (c) Response of the electromagnetic torque T_e. (d) Response of the command current i_a^* and measured current i_a.

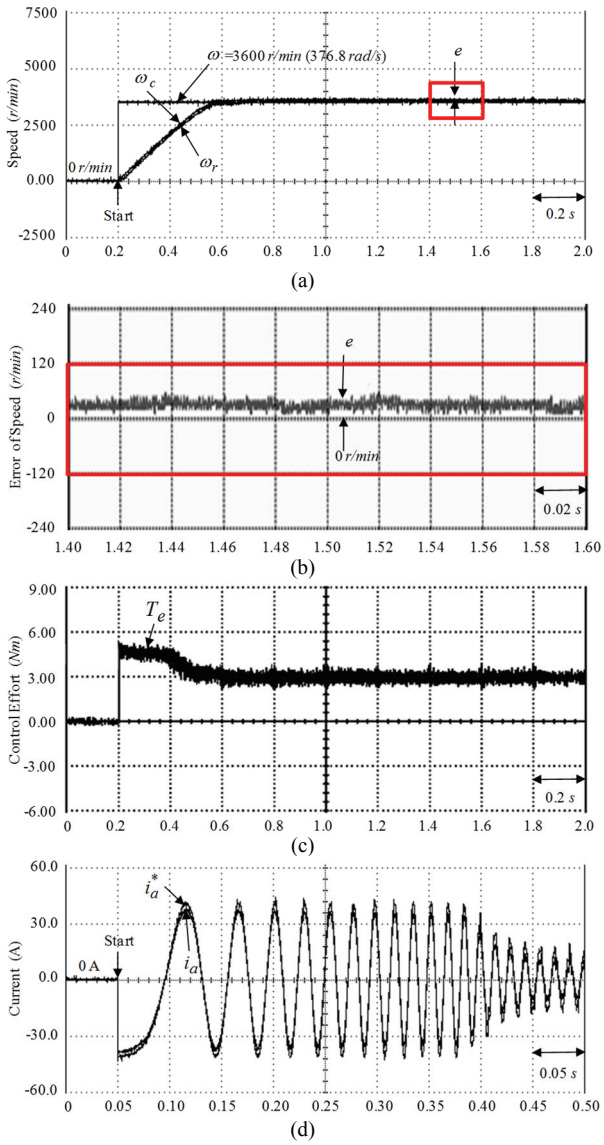

Fig. 10. Experimental results of the SynRM driving CVT system by means of the RGOPNN control system with two fixed learning rates in Case 2. (a) Tracking response of the rotor speed. (b) Zoomed response of the tracking error e. (c) Response of the electromagnetic torque T_e. (d) Response of the command current i_a^* and measured current i_a.

measured current i_a due to inappropriate regulation of the PI current controller and the action of a lot of viscous frictional forces, such as the wheel, the first pulley shaft, the second shaft-wheel side, the second shaft and the first pulley shaft-SynRM side.

These experimental results from the RGOPNN control system with two fixed learning rates show the sluggish tracking response of the speed for the SynRM driving CVT system. The weak robustness under a larger nonlinear disturbance occurs in the RGOPNN control system with two fixed learning rates due to inappropriately regulated learning rates.

Considering the prerequisites of stability in experimentation, all of the control gains of the ARGOPNN with a MPSO control system are chosen as $\beta = 0.32$ and $\zeta = 0.51$ to achieve the best transient control performance. The numbers of neurons of the input-hidden-output layers in the RGOPNN, as shown in Fig. 4, are 2-4-1. The computation time of the MPSO algorithm is 0.68 ms to obtain the two best solutions. The inertia weights, speeds of particles, positions of the particles and construction factors related to ARGOPNN with a MPSO are 0.42, 0.35, 0.18 and 0.11 for $\mu_{1,20}(t) = \mu_1^*(t)$; and 0.45, 0.31, 0.12 and 0.08 for $\mu_{2,20}(t) = \mu_2^*(t)$, respectively. A flowchart of the execution of the ARGOPNN

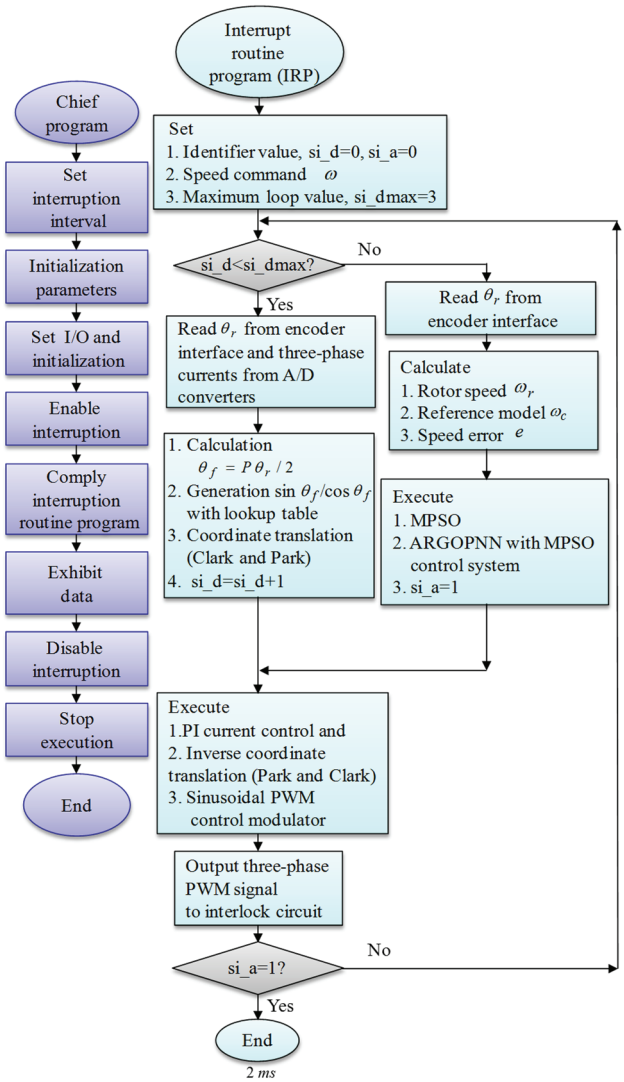

Fig. 11. Flowchart of the execution of the ARGOPNN with a MPSO control system by means of a DSP control system.

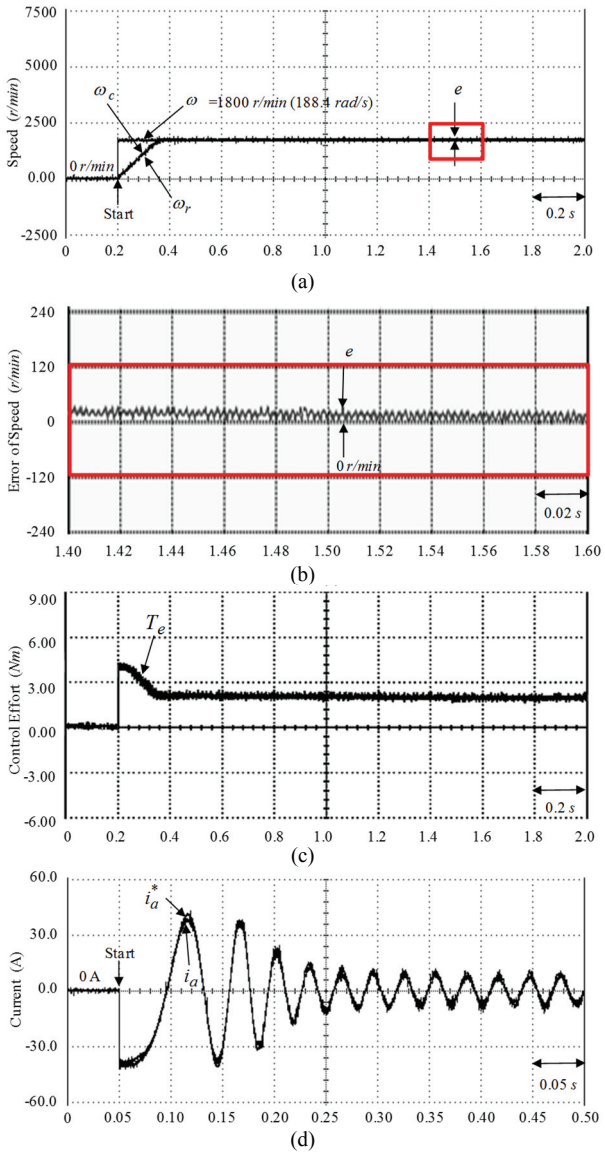

Fig. 12. Experimental results of the SynRM driving CVT system by means of the ARGOPNN with a MPSO control system in Case 1. (a) Tracking response of the rotor speed. (b) Zoomed response of the tracking error e. (c) Response of the electromagnetic torque T_e. (d) Response of the command current i_a^* and measured current i_a.

with a MPSO control system and real-time implementation by means of a DSP control system consists of a chief program and an interrupt routine program (IRP) as shown in Fig. 11.

First, some of the parameters and input/output (I/O) ports are initialized in the chief program. Then an interrupt interval with a 2 *ms* sampling interval for the interrupt routine program (IRP) is set. Next the interrupt is enabled. Some control data are then monitored by the chief program. The IRP is applied to read the rotor position of the SynRM driving CVT system from the encoder interface and the three-phase currents from the analog-to-digital (A/D) converter. It is also used to calculate the rotor position and speed, execute the lookup table and coordinate translation, execute the PI current control, execute the MPO and the ARGOPNN with a MPSO control system, and output execute the three-phase current commands to execute the sinusoidal PWM circuit for switching the 3-sets of IGBT power modules VSI via execute the interlock and isolated circuits. The 3-sets of IGBT power modules VSI is switched by execute the current-controlled sinusoidal PWM modulator with a switching frequency of 15 kHz.

The experimental results of the ARGOPNN with a MPSO control system for a SynRM driving CVT system in Case 1 and Case 2 are shown in Fig. 12 and Fig. 13, respectively.

Since low velocity operation has little disturbance, the speed tracking response shown in Fig. 12(a) has better tracking performance. Better tracking response of the speed is shown in Fig. 13(a) under the occurrence of a larger total unknown nonlinear load torque and twice the parameters variations. The tracking responses of the speed error e

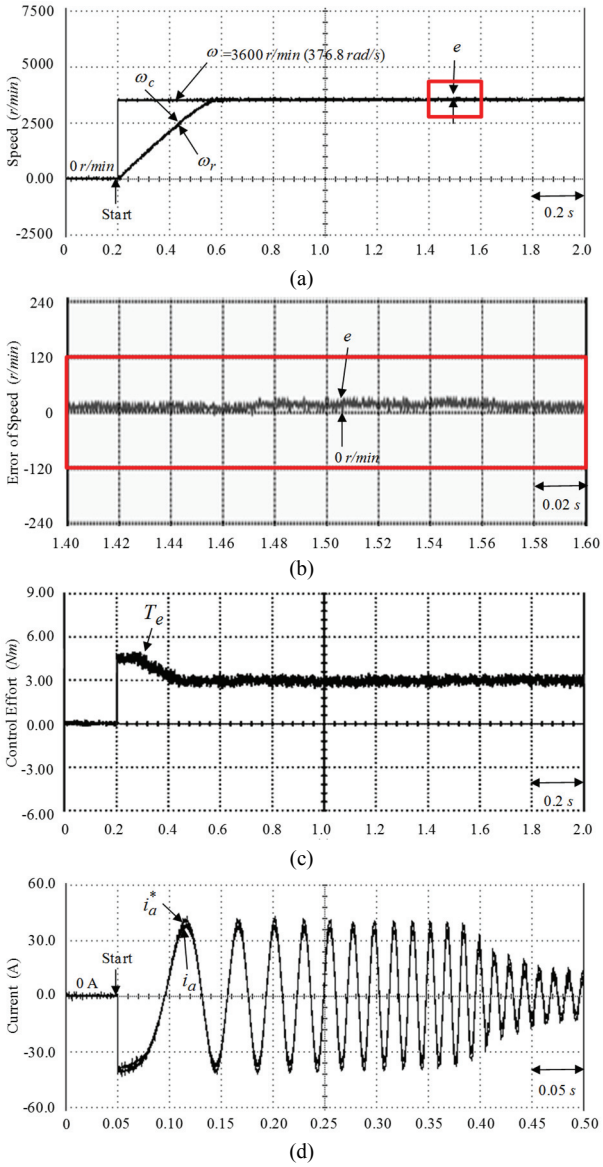

Fig. 13. Experimental results of the SynRM driving CVT system by means of the ARGOPNN with a MPSO control system in Case 2. (a) Tracking response of the rotor speed. (b) Zoomed response of the tracking error e. (c) Response of the electromagnetic torque T_e. (d) Response of the command current i_a^* and measured current i_a.

shown in Fig. 12(b) and Fig. 13(b) have little tracking error. The responses of the electromagnetic torque T_e shown in Fig. 12(c) and Fig. 13(c) also have little vibration. The tracking responses of the command current i_a^* and measured current i_a shown in Fig. 12(d) and Fig. 13(d) have better appearances. The low-speed operation was the same as the nominal case due to smaller disturbances. The speed tracking response in Fig. 13(a) shows a higher tracking performance under a larger total unknown nonlinear load torque and twice the parameters variations due to the online adaptive mechanism of the RGOPNN control with an adaptive law and the operation of

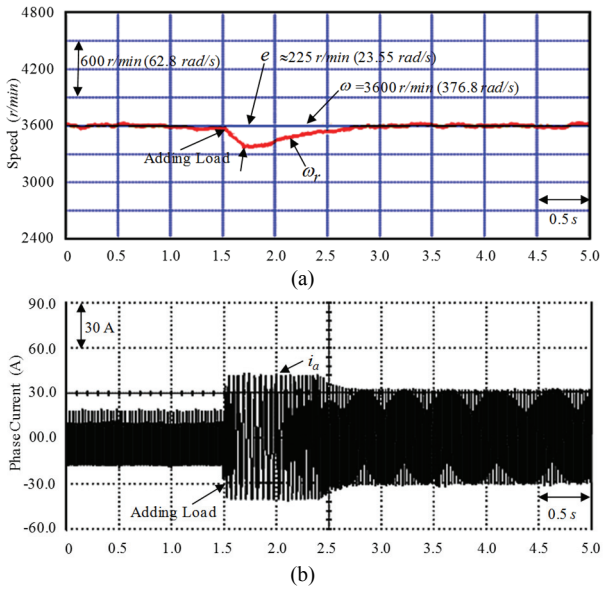

Fig. 14. Experimental results while adding a load disturbance and total unknown nonlinear load torque $T_1^l = 2Nm\,(T_l) + T_t$ at 3600 *r/min* (376.8 *rad/s*) when using the RGOPNN control system with two fixed learning rates. (a) Response of the speed regulation. (b) Response of the measured current i_a in phase *a*.

the remunerated controller with a reckoned law. Furthermore, the dynamic response of the electromagnetic torque T_e brings about a lower torque ripple by the online regulation of the RGOPNN to deal with the unmodelled dynamics of the CVT system. These nonlinear interferences are the V-belt shaking friction and drive friction from the first pulley side to the second pulley side. From the obtained experimental results, precise tracking performance can be acquired for the SynRM driving CVT system by means of the ARGOPNN with a MPSO control system due to the online adaptive mechanism of the RGOPNN control with an adaptive law and the remunerated controller with a reckoned law. Therefore, these experimental results demonstrate that the ARGOPNN with a MPSO control system result in better control performance than the RGOPNN control system with a fixed learning rate under high velocity interference for a SynRM driving a CVT system.

The measured rotor speed responses when adding a load disturbance and total unknown nonlinear load torque $T_1^l = 2Nm\,(T_l) + T_t$ tested using the RGOPNN control system with two fixed learning rates and the ARGOPNN with a MPSO control system. The obtained experimental result of a load adjustment by means of the RGOPNN control system with two fixed learning rates while adding load disturbance and total unknown nonlinear load torque $T_1^l = 2Nm\,(T_l) + T_t$ on a command rotor speed of 3600 *r/min* (376.8 *rad/s*) is shown in Fig. 14. The experimental result of a load adjustment using the ARGOPNN with a MPSO control

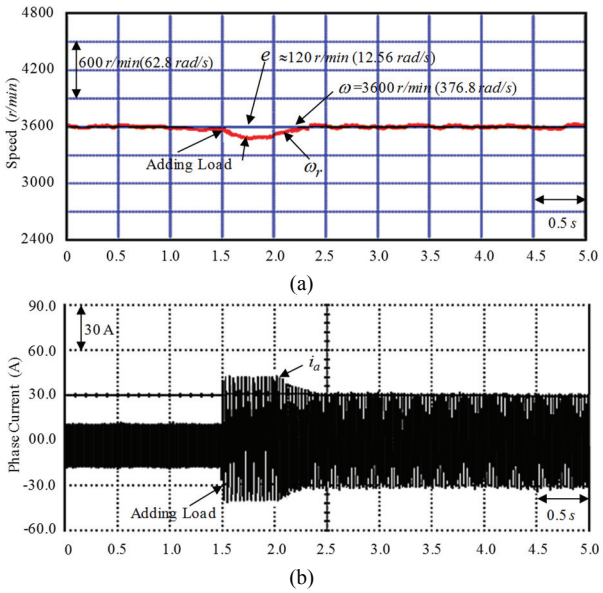

Fig. 15. Experimental results while adding a load disturbance and total unknown nonlinear load torque $T_1^l = 2Nm\ (T_l) + T_t$ at 3600 *r/min* (376.8 *rad/s*) when using of the ARGOPNN with a MPSO control system. (a) Response of the speed regulation. (b) Response of the measured current i_a in phase *a*.

system when adding a load disturbance and total unknown nonlinear load torque $T_1^l = 2Nm\,(T_l) + T_t$ on a command rotor speed of 3600 *r/min* (376.8 *rad/s*) is shown in Fig. 15. The degenerated responses under adding a load disturbance and total unknown nonlinear load torque $T_1^l = 2Nm\,(T_l) + T_t$ are greatly improved by using the ARGOPNN with a MPSO control system. Transient responses of the ARGOPNN with a MPSO control system have a faster convergence and better load regulation than the RGOPNN control system with two fixed learning rates.

Additionally, a comparison of the control performances of using the RGOPNN control system with two fixed learning rates and the ARGOPNN with a MPSO control system is presented in Table I with regard to the experimental results of three test cases. The maximum errors (ME) of e by means of the RGOPNN control system with two fixed learning rates for Case 1, Case 2 and under adding a load disturbance and total unknown nonlinear load torque $T_1^l = 2Nm\,(T_l) + T_t$ are 76 *r/min*, 93 *r/min* and 225 *r/min*, respectively. In addition, the root-mean-square errors (RMSE) of e by means of the RGOPNN control system with two fixed learning rates for Case 1, Case 2 and under adding a load disturbance and total unknown nonlinear load torque $T_1^l = 2Nm\,(T_l) + T_t$ are 33 *r/min*, 39 *r/min* and 32 *r/min*, respectively. The ME of e by means of the ARGOPNN with a MPSO control system for Case 1, Case 2 and under adding a load disturbance and total unknown nonlinear load torque $T_1^l = 2Nm\,(T_l) + T_t$ are 45 *r/min*, 76 *r/min* and 120 *r/min*, respectively. In addition, the RMSE of e by means of the ARGOPNN with a MPSO control system for Case 1, Case 2 and under adding a load disturbance and total unknown nonlinear load torque $T_1^l = 2Nm\,(T_l) + T_t$ are 22 *r/min*, 25 *r/min* and 21 *r/min*, respectively.

TABLE II
PERFORMANCE COMPARISON OF THE CONTROL SYSTEMS

Control System and Three Test Cases / Performance	RGOPNN Control System with Two Fixed Learning Rates		
	Case 1	Case 2	under adding load disturbance and total unknown nonlinear load torque $T_1^l = 2Nm\ (T_l) + T_t$ case
ME of e	76 *r/min* (7.9 *rad/s*)	93 *r/min* (9.7 *rad/s*)	225 *r/min* (23.6 *rad/s*)
RMSE of e	33 *r/min* (3.5 *rad/s*)	39 *r/min* (4.1 *rad/s*)	32 *r/min* (3.3 *rad/s*)
Control System and Three Test Cases / Performance	ARGOPNN with MPSO Control System		
	Case 1	Case 2	under adding load disturbance and total unknown nonlinear load torque $T_1^l = 2Nm\ (T_l) + T_t$ case
ME of e	45 *r/min* (4.7 *rad/s*)	76 *r/min* (7.9 *rad/s*)	120 *r/min* (12.56 *rad/s*)
RMSE of e	22 *r/min* (2.3 *rad/s*)	25 *r/min* (2.6 *rad/s*)	21*r/min* (2.2 *rad/s*)

TABLE III
PROPERTY PERFORMANCE COMPARISON OF THE CONTROL SYSTEMS

Control System / Property Performance	RGOPNN Control System with Two Fixed Learning Rates	ARGOPNN with MPSO Control System
Dynamic Response	Fast	Faster
Load Regulation apability	Better	Best
Convergence Speed	Fast	Faster

Table II shows that the ARGOPNN with a MPSO control system results in a little tracking error in comparison with the RGOPNN control system with two fixed learning rates. In accordance with the measurements listed in Table II, the ARGOPNN with a MPSO control system brings about beneficial control performance.

Furthermore, some property performance comparisons for the RGOPNN control system with two fixed learning rates and the ARGOPNN with a MPSO control system are presented in Table III on the basis of experimental results. In Table III, some of the performances of the ARGOPNN with a MPSO control system are advantageous when compared to the RGOPNN control system with two fixed learning rates.

V. CONCLUSION

A SynRM driving system has been smoothly applied in a CVT system by use of the ARGOPNN with a MPSO control system. The chief contributions of this paper are listed below. 1) Dynamic models of the SynRM driving CVT system were originated. 2) The ARGOPNN control system made up of a censor controller, the RGOPNN controller with an adaptive law and the remunerated controller with a reckoned law have been favorably proposed for smoothing the control effort and enhancing the robustness of a system when uncertainties exist. 3) The adaptive law of the online parameters has been successfully used in the RGOPNN control in accordance with the Lyapunov stability theorem. 4) The adaptive regulation mechanics of two learning rates in the two weights of the RGOPNN control with a MPSO have been applied in the ARGOPNN control system to achieve a rapid convergence. Finally, the proposed ARGOPNN with a MPSO control system is more advisable than the RGOPNN control system with two fixed learning rates for a SynRM driving CVT system in terms of control performance.

ACKNOWLEDGMENT

The author would like to acknowledge the financial support of the Ministry of Science and Technology of Taiwan under grant MOST 107-2221-E-239-021.

REFERENCES

[1] W. Chai, W. Zhao, and B. Kwon, "Optimal design of wound field synchronous reluctance machines to improve torque by increasing the saliency ratio," *IEEE Trans. Magn.*, Vol. 53, No. 11, Art. No. 8206604-4, 2017.

[2] G. Artetxe, J. Paredes, B. Prieto, M. Martinez-Iturralde, and I. Elosegui, "Optimal pole number and winding designs for low speed–high torque synchronous reluctance machines," *Energies*, Vol. 11, No.1, 128, Jan. 2018.

[3] T. Matsuo, A. E. Antably, and T. A. Lipo, "A new control strategy for optimum-efficiency operation of a synchronous reluctance motor," *IEEE Trans. Ind. Appl.*, Vol. 33, No. 5, pp. 1146-1153, Sep./Oct. 1997.

[4] E. M. Rashad, T. S. Radwan, and M. A. Rahman, "A maximum torque per ampere vector control strategy for synchronous reluctance motors considering saturation and iron losses," *IEEE Ind. Appl. Conf.,* pp. 2411-2417, 2004.

[5] L. Guzzella and A. M. Schmid, "Feedback linearization of spark-ignitionengines with continuously variable transmissions," *IEEE Trans. Contr. Syst. Technol.*, Vol. 3, No. 1, pp. 54-58, Feb. 1995.

[6] W. Kim and G. Vachtsevanos, "Fuzzy logic ratio control for a CVT hydraulic module," *Proc. of the IEEE Symp. Intelligent Control*, pp. 151-156, 2000.

[7] C. Y. Tseng, Y. F. Lue, Y. T. Lin, J. C. Siao, C.H. Tsai, and L. M. Fu, "Dynamic simulation model for hybrid electric scooters," *IEEE Int. Symp. Industrial Electronics*, pp. 1464-1469, 2009.

[8] G. Carbone, L. Mangialardi, B. Bonsen, C. Tursi, and P. A. Veenhuizen, "CVT dynamics: Theory and experiments," *Mechanism and Machine Theory*, Vol. 42, No. 4, pp. 409-428, Apr. 2007.

[9] K. S. Narendra and K. Parthasarathy, "Identification and control of dynamical system using neural networks," *IEEE Trans. Neural Netw.*, Vol. 1, No. 1, pp. 4-27, Mar. 1990.

[10] P. S. Sastry, G. Santharam and K. P. Unnikrishnan, "Memory neural networks for identification and control of dynamical systems," *IEEE Trans. Neural Netw.*, Vol. 5, No. 2, pp. 306-319, Jun. 1994.

[11] C. H. Lin, "A PMSM driven electric scooter system with V-belt continuously variable transmission using novel hybrid modified recurrent Legendre neural network control," *J. Power Electron.,* Vol. 15, No. 1, pp. 220-229, Jan. 2015.

[12] C. H. Lin, "A backstepping control of LSM drive systems using adaptive modified recurrent Laguerre OPNNUO," *J. Power Electron.*, Vol. 16, No. 2, pp. 598-609, Mar. 2016.

[13] J. C. Ting and D. F. Chen, "Nonlinear backstepping control of SynRM drive systems using reformed recurrent Hermite polynomial neural networks with adaptive law and error estimated law," *J. Power Electron.,* Vol. 18, No. 5, pp. 1380-1397, Sep. 2018.

[14] J. C. Ting and D. F. Chen, "SynRM servo-drive CVT systems using MRRHPNN control with mend ACO," *J. Power Electron.,* Vol. 18, No. 5, pp. 1409-1423, Sep. 2018.

[15] C. Wu, H. Zhang and T Fang, "Flutter analysis of an airfoil with bounded random parameters in incompressible flow via Gegenbauer polynomial approximation," *Aerospace Sci. Technol.*, Vol. 11, No. 7-8, pp. 518-526, Nov./Dec. 2007.

[16] Y. Zhang and W. Li, "Gegenbauer neural network and its weights-direct determination method," *IET Electron. Letters,* Vol. 45, No. 23, pp. 1184-1185, Nov. 2009.

[17] C. H. Lin, "A six-phase CRIM driving CVT using blend modified recurrent Gegenbauer OPNN Control," *J. Power Electron.*, Vol. 16, No. 4, pp. 1438-1454, Jul. 2016.

[18] C. H. Lin, "Comparative dynamic control for continuously variable transmission with nonlinear uncertainty using blend amend recurrent Gegenbauer-functional-expansions neural network," *Nonlinear Dynamics*, Vol. 87, No. 3, pp. 1467-1493, Feb. 2017.

[19] C. H. Lin and C. Y Yu, "Blend recurrent Gegenbauer OPNNAPSO control for a SynRM servo-drive CVT system," *Proc. IEEE Conf. Industrial Electronics and Applications*, Wuhan, China, pp. 1060-1065, 2018.

[20] J. Kennedy and R. Eberhart, "Particle swarm optimization," *Proc. IEEE Int. Conf. Neural Networks,* Perth, WA, pp. 1942-1948, 1995.

[21] M. Clerc and J. Kennedy, "The particle swarm-explosion, stability, and convergence in a multi-dimensional complex space," *IEEE Trans. Evol. Comput.*, Vol. 6, No. 1, pp. 58-73, Feb. 2002.

[22] Y. Shi and R. C. Eberhart, "A modified particle swarm optimizer," *Proc. IEEE Int. Conf. Evolutionary Computation,* Anchorage, Alaska, pp. 69-73, 1998.

[23] R. Akbari and K. Ziarati, "A rank based particle swarm optimization algorithm with dynamic adaptation," *J. Computational Appl. Mathematics*, Vol. 235, No. 8, pp. 2694-2714, Feb. 2011.

[24] C. H. Lin, "Composite recurrent Laguerre orthogonal polynomials neural network dynamic control for continuously

variable transmission system using altered particle swarm optimization," *Nonlinear Dynamics*, Vol. 81, No. 3, pp. 1219-1245, Aug. 2015.
[25] J. J. E. Slotine and W. Li, *Applied Nonlinear Control.* Prentice Hall, Englewood Cliffs, New Jersey, 1991.
[26] K. J. Astrom and B. Wittenmark, *Adaptive Control*, Addison Wesley, New York, 1995.

Chih-Hong Lin received his B.S. and M.S. degrees in Electrical Engineering from the National Taiwan University of Science and Technology, Taipei, Taiwan, ROC, in 1989 and 1991, respectively. He received his Ph.D. degree in Electrical Engineering from the Chung Yuan Christian University, Taoyuan, Taiwan, ROC, in 2001. He is presently working as a Professor in the Department of Electrical Engineering, National United University, Miaoli, Taiwan, ROC. His current research interests include power electronics, motor servo drives and intelligent control.

Kuo-Tsai Chang was born in Taiwan, ROC, in 1964. He received his MS degree from the Department of Electrical Engineering, National Taiwan University of Science and Technology, Taipei, Taiwan, ROC, in 1991; and his Ph.D. degree from the Department of Engineering and System Science, National Tsing Hua University, Hsinchu, Taiwan, ROC, in 2002. From 1991 to 2002, he was a Lecturer in the Department of Electrical Engineering, National Lien-Ho Institute of Technology, Miaoli, Taiwan, ROC. Since 2007, he has been a Professor in the Department of Electrical Engineering, National United University, Miaoli, Taiwan, ROC. His current research interests include power electronics, motor control and ultrasonic engineering.